Dual-Frequency Transducer for Nonlinear Contrast Agent Imaging

Axel Guiroy, Anthony Novell, *Member, IEEE*, Erling Ringgaard, Rasmus Lou-Moeller, Jean-Marc Grégoire, André-Pierre Abellard, Tomasz Zawada, Ayache Bouakaz, *Senior Member, IEEE*, and Franck Levassort

***Abstract*—Detection of high-order nonlinear components issued from microbubbles has emerged as a sensitive method for contrast agent imaging. Nevertheless, the detection of these high-frequency components, including the third, fourth, and fifth harmonics, remains challenging because of the lack of transducer sensitivity and bandwidth. In this context, we propose a new design of imaging transducer based on a simple fabrication process for high-frequency nonlinear imaging. The transducer is composed of two elements: the outer low-frequency (LF) element was centered at 4 MHz and used in transmit mode, whereas the inner high-frequency (HF) element centered at 14 MHz was used in receive mode. The center element was pad-printed using a lead zirconate titanate (PZT) paste. The outer element was molded using a commercial PZT, and curved porous unpoled PZT was used as backing. Each piezoelectric element was characterized to determine the electromechanical performance with thickness coupling factor around 45%. After the assembly of the two transducer elements, hydrophone measurements (electroacoustic responses and radiation patterns) were carried out and demonstrated a large bandwidth (70% at −3 dB) of the HF transducer. Finally, the transducer was evaluated for contrast agent imaging using contrast agent microbubbles. The results showed that harmonic components (up to the sixth harmonic) of the microbubbles were successfully detected. Moreover, images from a flow phantom were acquired and demonstrated the potential of the transducer for high-frequency nonlinear contrast imaging.**

I. Introduction

Contrast enhanced ultrasound is now widely used in cardiology and radiology [1]. Ultrasound contrast agents consist of microbubbles which are intravenously injected to enhance the echo from the blood flow. Currently, most contrast agent imaging strategies are based on the specific nonlinear scattering properties of the microbubbles. The microbubble nonlinear signature is used to discriminate between the echoes from tissue from those of contrast agent [2]. For many years, particular interest was drawn to the subharmonic component generated by the microbubbles [3], [4]. This particular frequency component appears at half of the transmitted frequency in the bubble vibration. Even if the subharmonic components are more difficult to observe, subharmonic imaging could present various advantages, such as the possibility to explore deeper organs because of lower attenuation and the absence of nonlinear contamination from tissues [3], [5]. Many investigations have also been performed on higher harmonic components generated by the microbubbles (third, fourth, and fifth harmonics) [6], [7], termed superharmonics. At these higher frequencies, the nonlinear propagation in tissues is weaker, thus providing a significant increase in the contrast detection (usually termed CTR, for contrast-to-tissue ratio) [6]. Although the level of each higher harmonic component generated by microbubbles is weaker than that at the second harmonic frequency, the loss of the SNR is largely compensated in superharmonic imaging by the contribution of several frequency components (in this example: third, fourth, fifth, and sixth). In the superharmonic imaging mode, the main challenge lies in using a transducer able to transmit at a low frequency and to receive sufficient superharmonic energy. In this context, we propose the development of a specific dual-frequency transducer able to transmit and receive at low- (LF) or high-frequency (HF).

Several dual-frequency transducers have already been realized for different contrast imaging applications. In 2008, Kim *et al.* proposed a dual-frequency transducer for second-harmonic imaging [8]. This two-element transducer was designed using lapped lithium niobate as the piezoelectric material. The operating LF was chosen at 20 MHz, and the HF at 40 MHz. The same year, Masoy *et al.* designed a five-element annular array (1–3 piezocomposites) for second-order ultrasound field (SURF) imaging using an LF element centered at 0.9 MHz for microbubble radial modulation (outer ring) while four inner HF elements were used at 7.5 MHz for imaging [9]. For this imaging modality, a significant difference of center frequencies is required (a factor between 7 and 10).

In 2010, a specific interleaved phased-array transducer was designed for superharmonic imaging [10]. The probe was composed of 44 LF elements used in transmit at 1 MHz while 44 HF elements were used in receive mode at 3.7 MHz. With a complex design and fabrication process, the transducer showed good suitability for superharmonic, harmonic, and subharmonic imaging. The same year, a

Manuscript received April 29, 2013; accepted August 19, 2013. This work was funded by the French Research Agency (ANR HYPERCAMPUS Mat&Pro and THERANOS) and European Union (FEDER Funds).

A. Guiroy, A.-P. Abellard, and F. Levassort are with Université François-Rabelais de Tours, GREMAN UMR7347 CNRS, Tours, France (e-mail: levassort@univ-tours.fr).

A. Novell, J. M. Grégoire, and A. Bouakaz are with UMR Inserm U930, Université François-Rabelais de Tours, PRES Centre, Val de Loire Université, Tours, France.

E. Ringgaard, R. Lou-Moeller, and T. Zawada are with MEGGITT A/S, Kvistgaard, Denmark.

*A. Guiroy and A. Novell have contributed equally to this work.

DOI http://dx.doi.org/10.1109/TUFFC.2013.2862

complete study by Gessner et *al.*, was published, describing a confocal imaging probe (with 2.5-MHz transmitter and 30-MHz receiver) for *in vivo* microvascular blood flow imaging [11].

In the present research study, the main objective is to design and to describe a simple fabrication process for an efficient dual-frequency transducer. The transducer is composed of two curved elements prefocused at 12.5 mm. The center frequency of the HF element is at 14 MHz and the LF element frequency is selected around 4 MHz. Because of the frequency range chosen, applications such as breast cancer detection are targeted. The design and fabrication of the transducer is described in the next section. Then, the electromechanical (thickness-mode) performances of the two elements are evaluated and the electroacoustic response and radiation patterns of the transducer are measured. Experimental results are compared with theory using a hybrid numerical model (finite difference–pseudo spectral time domain, FD-PSTD [12], [13]) to calculate the pressure field in front of the transducer in water. Finally, the transducer was tested to estimate its efficiency for contrast agent detection in superharmonic imaging mode, and nonlinear imaging mode is shown.

II. Design and Fabrication

A. Design

The dual-element structure was composed of two separate transducers assembled in one housing. Special attention was paid to the positioning of the two elements, and the same beam axis and focal distances were chosen. For that, an electrode backing with a curved top face was used to directly deposit the center element with a pad-printing process to deliver a curved piezoelectric thick film with the same radius of curvature. Pad-printing is an efficient and low-cost process adapted to piezoelectric thick film by Meggitt A/S (Kvistgaard, Denmark; http://ferroperm-piezo.com/). This process is particularly interesting for the deposition of thick film on a nonplanar structure. Moreover, it was reported that pad-printed thick film are suitable for both imaging (high bandwidth) and therapy (high sensitivity) [14], [15].

On the other hand, a curved ring (outer element) was previously fabricated with a standard route and glued onto the backing. The common focal distance is 12.5 mm. The schematic transducer structure with the constitutive elements is shown in Fig. 1. The center element was also designed to be used independently for medical imaging (transmit/receive mode) and a center frequency of 14 MHz was chosen. The inner disk is used as an HF element because for a ring-shaped element with a similar diameter, higher side lobes could be generated [8], [16]. To meet these requirements, the chosen focal distance is well adapted for the targeted applications such as breast imaging. A diameter of 4.4 mm was retained to deliver an f-number of 2.9 (typical values for our application are

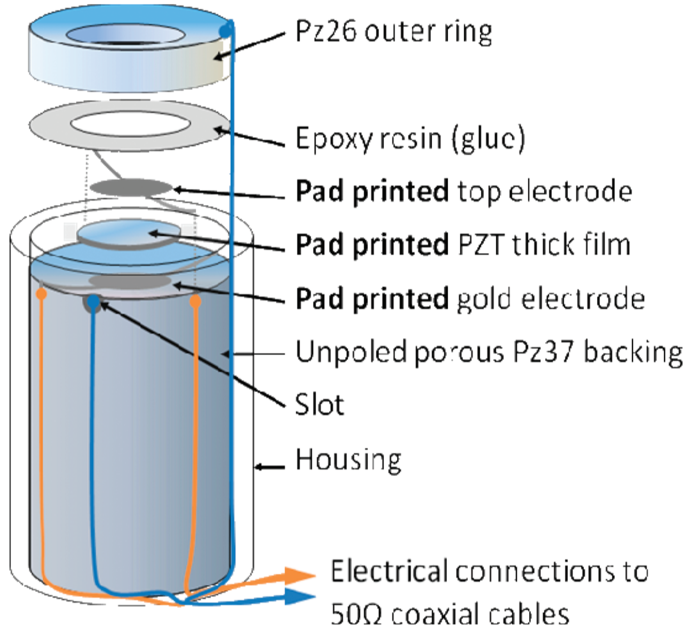

Fig. 1. Schematic representation of the dual-frequency transducer.

in the range 2 to 3). Moreover, according to the retained frequency, the expected depth of field and lateral resolution at −3 dB are around 5 mm and 300 μm, respectively. Finally, a high fractional bandwidth is needed and a minimum value of 60% at −6 dB is necessary for nonlinear imaging. This large bandwidth allowed coverage of several harmonic components (from 8 to 18 MHz).

For superharmonic imaging, the center frequency of the outer ring was chosen at 4 MHz to be consistent with the frequency range of microbubble activation. In fact, when microbubbles are excited close to their resonance frequency, strong nonlinear oscillations are induced, resulting in the generation of several higher harmonic components. For most commercial ultrasound contrast agents, the resonance frequency ranges between 1.5 and 5 MHz [17], [18]. In the focal zone, because of the large external diameter, the depth of field was shorter (expected at around 3.5 mm) but lateral resolution was similar (expected at around 300 μm) than the same properties of the HF element. For this element, the sensitivity was emphasized at the expense of the bandwidth to maximize the pressure values in the focal zone.

Finally, for each element, two connectors were added for independent use in receive, transmit, or dual modes.

B. Fabrication

The backing was made of porous unpoled lead zirconate titanate (PZT) based on Ferroperm Pz37 composition (Meggitt A/S) [19]. This porous material offers several advantages for transducer properties (in particular for the center element) [20]. Its thermal deformation is comparable to that of a thick film, which minimizes the appearance of cracks in the film during sintering. Moreover, the porosity content introduces relatively high acoustic attenuation (to be considered as a semi-infinite medium while minimizing its size), and finally, its acoustical impedance is high and close to the thick film, thus providing a large bandwidth for the transducer. A cylinder with a diameter of 14 mm was first fabricated and the top face was machined to have a spherical depression with a radius of curvature of 12.5 mm (which corresponds to the desired focal distance of the transducer).

The main steps of the pad-printing process for the fabrication of the center HF element (which can be used in both transmit and receive modes) are depicted in Fig. 2. First, the rheological properties of a Navy type-I paste initially used for screen printing were adapted (TF2100, InSensor, Kvistgaard, Denmark [21]). Here, PZT-based composition was used because of its high piezoelectric response.

A cliché was specifically fabricated into a steel plate with the desired lateral dimensions [Fig. 2(a)]. This cliché was filled with PZT paste and the excess was removed with a doctor blade [Fig. 2(b)]. Then the paste contained in the cliché was transferred onto the curved substrate with the silicon pad [Fig. 2(c) and (d)]. Several layers were successively deposited to reach the desired thickness which can be well controlled. Finally, the thick film was sintered and poled [14] to deliver a final thickness of 43 μm.

Previously, a gold bottom electrode was deposited with the same pad-printing process on the curved porous backing using commercial gold paste. Two gold-coated slots

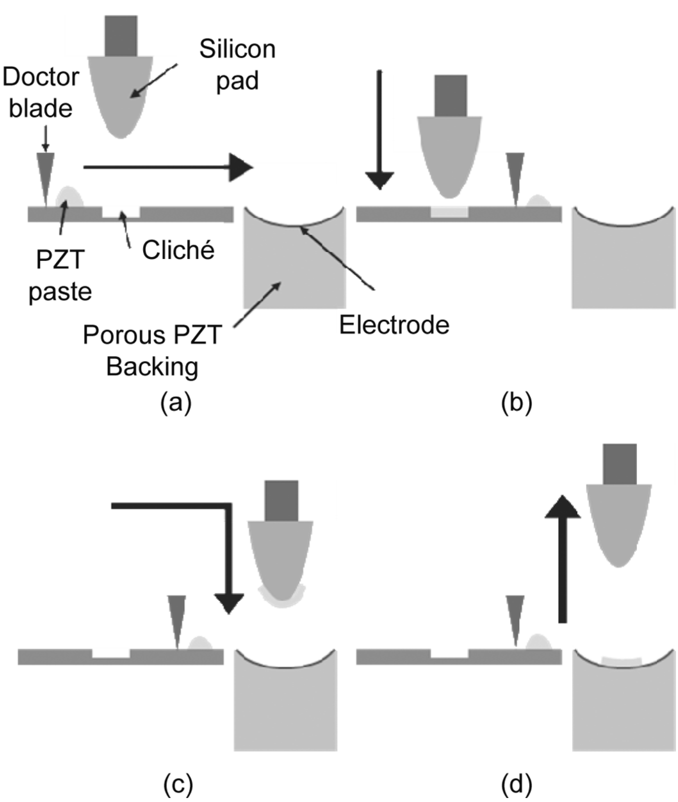

Fig. 2. Illustration of the pad printing technology.

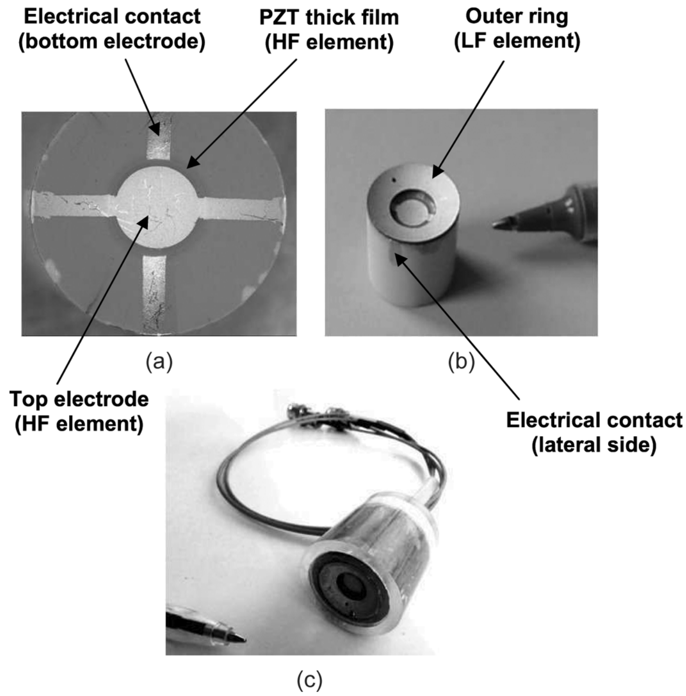

Fig. 3. Photographs of (a) top view of the structure after the deposition of the pad-printed center element, (b) structure after the bonding of the outer ring, (c) the final transducer.

from this circular bottom electrode were added to the lateral side of the porous backing for the electrical contacts (Fig. 1). For the top electrode and the two corresponding slots, commercial silver paste was used and deposited with the same process. The diameter of the thick film was slightly greater than that of the two electrodes to avoid electrical short-circuits (in particular during the poling step). Fig. 3(a) is a photograph of this intermediate structure (top view).

For superharmonic imaging, the LF element (outer ring) is used in transmit only where the sensitivity is of a primary interest. Because of the chosen center frequency (i.e., 4 MHz), thick-film technology is not suitable, and thus a standard bulk process was used for the fabrication. Ferroperm Pz26 (Ferroperm Piezoceramics AS, Kvistgaard, Denmark; http://ferroperm-piezo.com/) composition was used and a curved ring shape was obtained by machining. This ring was glued with epoxy resin [Fig. 3(b)]. The thickness of this layer was controlled to be sufficiently thick to first deliver electrical insulation between electrodes (slots) of the center element and this ring (Fig. 1). The acoustic impedance of the epoxy resin is low compared with the porous PZT backing and contributes to modification of the trade-off between bandwidth and sensitivity. In this case, the sensitivity is significantly improved at the expense of bandwidth. The thickness of this polymer layer was estimated at 500 μm.

From the four electrical contacts on the lateral side of the backing, two 50-Ω coaxial cables were soldered for each element. A shielded housing was added to finish the transducer [Fig. 3(c)].

III. Experimental Procedure

A. Characterization Methods

1) Electrical Impedance Measurements of Piezoelectric Elements: An HP4395A spectrum analyzer (Agilent Technologies Inc., Santa Clara, CA) with its impedance test kit and specific spring clip fixture was used to measure the electrical impedance of the two piezoelectric elements around the fundamental resonance thickness mode. This allowed deduction of the dielectric, mechanical, and piezoelectric parameters for the corresponding mode. These measurements were performed before the assembly of the transducer. Thus, the LF element was directly characterized in free mechanical conditions (in air), whereas the pad-printed HF element was characterized on the backing.

With an equivalent electrical circuit model (here, the Krimholtz–Leedom–Matthaei (KLM) model was used [22]–[24]), calculated impedances were obtained and used to fit experimental data and to deliver the thickness-mode parameters.

The HF element is included in a structure containing four layers (porous PZT backing, bottom gold electrode, pad-printed thick film, and top silver electrode). Thus, the three inert layers are taken into account in the KLM scheme (i.e., thickness, density, and mechanical properties) to deduce only the thick-film parameters [25], [26]. For electrode materials, data are taken from [27], where attenuation was neglected, whereas for the porous PZT substrate, longitudinal wave velocity was measured by a transmission method with a commercial transducer with a center frequency at 10 MHz and the density was deduced from Archimedes method. Moreover, a cross section of an identical structure was made and SEM analysis was performed to deduce the thickness (of all layers) and the volume porosity content (porous PZT backing), which was evaluated to be 15%.

2) Acoustical Measurements: The transducer was immersed in degassed/deionized water tank and hydrophone measurements were performed with a 0.2-mm needle hydrophone (Precision Acoustics Ltd., Dorchester, UK) mounted on an XYZ positioning system (TriOptics GmbH, Wedel, Germany) to deduce radiated pressure. For each of the LF and HF elements, an excitation signal of 10-cycle burst at the corresponding center frequency was generated using Matlab (The MathWorks Inc., Natick, MA) and then transmitted through a GPIB port (National Instruments Corp., Austin, TX) to an arbitrary function generator (33220A, Agilent Technologies Inc.). The signal was then amplified using a power amplifier (150A100B, Amplifier Research Corp., Souderton, PA) and transmitted to the transducer. The propagated signals as received on the hydrophone from both LF and HF elements (one after the other) were displayed on a digital oscilloscope (Tektronix Inc., Beaverton, OR) and the radiation patterns of each element were determined. Thus, the focal distance, lateral resolutions, and depth of field were estimated. Moreover, using a one-cycle burst at the center frequency of each element as the excitation waveform, electroacoustic responses were measured at the focal distance and bandwidths and axial resolutions were measured.

B. Transducer Model

A 3-D axisymmetrical model based on a hybrid FD-PSTD [13] method was used. In this study, this model was specifically adapted to curved piezoelectric thick film configurations to calculate first the pressure field in a plane in front of the transducer (near field). In a second step, the DREAM Toolbox [28] used the pressure in this plane as input data to calculate the corresponding radiation pattern in water (in particular, in the focal zone). Calculations were performed independently for the two transducer elements.

1) FD-PSTD Model: This approach combined a pseudo-spectral time-domain (PSTD) algorithm with a finite-difference (FD) approximation. Pseudospectral methods were first introduced by Kreiss and Oliger [29] and Wojcik et *al.* [30] applied it to acoustic wave propagation. This numerical method delivers a good numerical stability and a small number of required nodes per wavelength [31], [32]. Moreover, perfectly matching layers (PMLs) [33], [34] are often combined with PSTD algorithms. This theory was extended to piezoelectric materials, integrating electric excitation to simulate both the piezoelectric transducer vibration and the resulting wave propagation in the surrounding medium. The quasi-static approximation was used for the piezoelectric material which leads to using the finite-difference method (to solve an equation with a second-order derivative that is not time-dependent) to calculate the electrical potential inside the piezoelectric medium. This unified model (FD-PSTD) takes advantages of both methods and was first validated by successful comparisons with FEM software [12], [35], modeling the behavior of a piezoelectric disk immersed in water and a transducer in simple 2-D configurations. To improve the potential and use of this hybrid model, a 3-D axisymmetrical version was developed and applied to high-frequency lens transducer simulations [13]. In this present work, this last version was used with a new detail in which the curvature of the piezoelectric thick film is taken into account. With the axisymmetry condition, the 3-D space is reduced to 2-D space, which is discretized with a constant step. Fig. 4 shows the transition from the dual-frequency transducer configuration to the 2-D discretized space (only for the center element on Fig. 4) for the calculation. A four-layer structure is simulated with the backing, top and bottom electrodes, and the curved thick film. The grid includes nodes where mechanical, dielectric, and piezoelectric properties are initially known. The calculation is performed in three main steps previously described in [13]. For the initial conditions, stress (T), strain (S), and electric field (E) are null in the calculation space and an electric field is created inside the curved thick film by

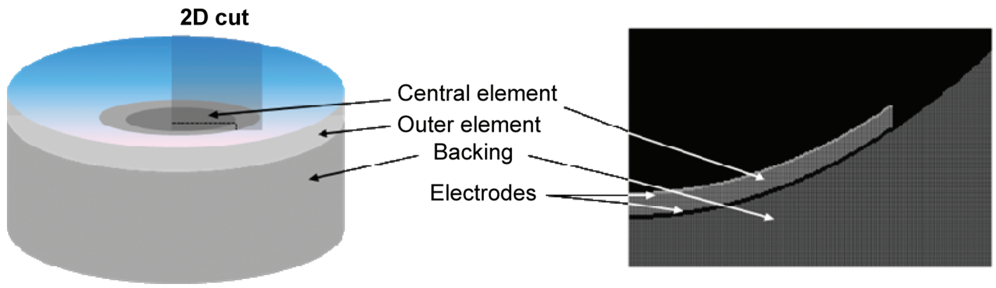

Fig. 4. Schematic representation of the transition from 3-D transducer configuration to 2-D model mesh (with only the center element).

a sine wave electrical excitation (with several cycles of a frequency corresponding to the center frequency of each element). This is a recursive algorithm and from the calculation of the stress field at time t, the temporal derivatives of acoustic velocity are obtained by solving relation 1 in Fig. 5. By using the fourth-order Adams–Bashforth (AB) relationship, the time integration is performed to deduce the acoustic velocity field (v). The second step consists of solving relation 2 in Fig. 5 with the FD method to deduce the temporal derivative of the electric field [or the electric field (E) with AB time integration]. Third, the stress tensor (T) is calculated at $t + \Delta t$ using successively relation 3 in Fig. 5 and AB time integration. Then, a new iteration can begin. For the simulations, all of the optimized criteria already described in [12] and [13], such as spatial steps and temporal increment, are applied. For the propagation in the front homogeneous media (here, water), all is performed with the same algorithm and pressure values are calculated at each node.

2) DREAM Toolbox: The DREAM toolbox is an analytic model using the Rayleigh integral expression to obtain the space impulse response (SIR) of a point source for simulating acoustic field propagation in a homogeneous medium [28]. The corresponding radiated source is assumed to be a planar rigid piston with a uniform normal velocity over the source. Having SIR at $z = h$ (value for example along the z-axis, Fig. 6), the pressure radiated by a piston at $z = h$ can be obtained by convoluting its acceleration (a) at $z = 0$ [$a(x,t,z = 0) = (\partial^2 u(x,t,z = 0))/\partial t^2$, where u is the displacement] with SIR at $z = h$ (Fig. 6):

$$p(x,t,z = h) = \rho \cdot \mathrm{SIR}(x,t,z = h) * a(x,t,z = 0). \quad (1)$$

Previously, the pressure field was calculated for each node of the grid in near field with the FD-PSTD method until the represented plane (dashed line) on Fig. 6. At each node of this plane, planar radiated sources are considered. Finally, a summation of all these contributions allows deduction of the acoustic response of the transducer in this half-space.

This calculation could also be done with the PS-FDTD model but a propagation at large scale in a homogeneous medium (here, water) is more efficient with the analytical model, which is less time consuming.

C. Contrast Agent Detection

The transducer was evaluated for superharmonic component detection. For this experiment, a long pulse was transmitted to extract each of the frequency components. The LF transducer was excited with a 20-cycle burst at 3 MHz using a driving acoustic pressure of 500 kPa (non-derated mechanical index = 0.29). The HF element

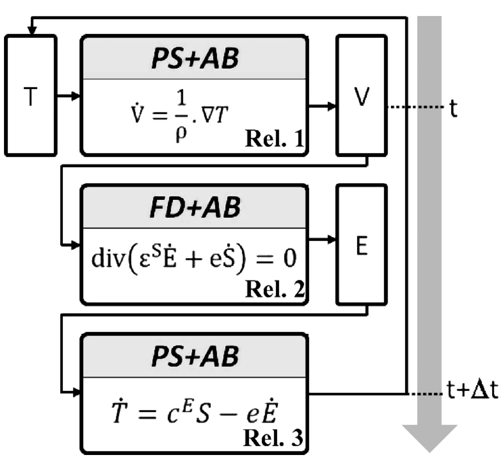

Fig. 5. Steps of FD-PSTD algorithm (ε^{S} = tensor of the dielectric constant at constant strain, e = piezoelectric tensor, and c^{E} = elastic tensor at constant electric field).

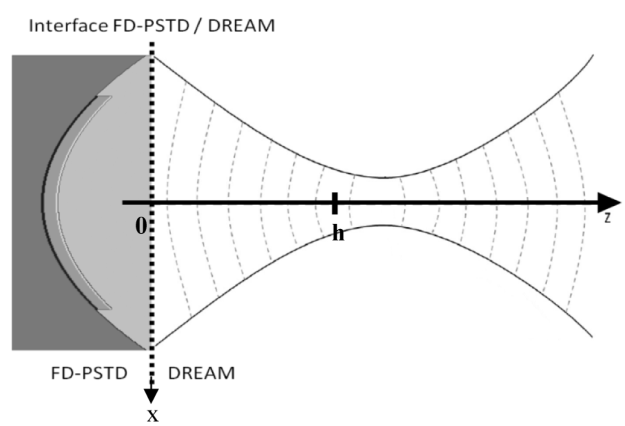

Fig. 6. Link between FD-PSTD model and DREAM toolbox: acoustic field in front of transducer (center element only) is obtained with FD-PSTD (until the plane in dashed line) and DREAM toolbox is used for propagation.

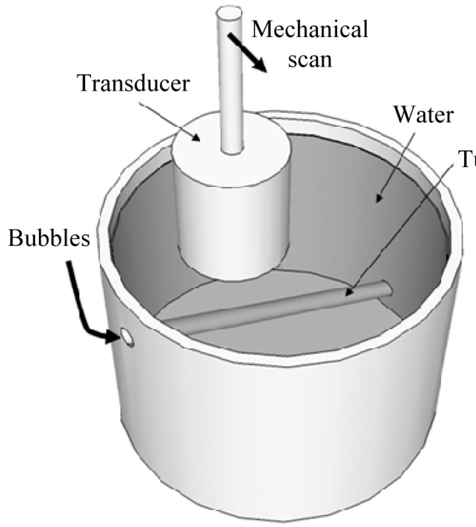

Fig. 7. Schematic drawing of the experimental setup for superharmonic imaging with a flow phantom.

was used in receive mode to collect the higher harmonic components. Echoes from a linear reflector (50-µm copper wire) were first recorded. Echoes were averaged on 16 measurements. Furthermore, superharmonic imaging was performed on a flow phantom containing a 0.6-mm-diameter tube in which the solution of BR14 microbubbles (Bracco Research, Geneva, Switzerland) was injected into a reservoir at a dilution of 1/2000 and circulated at a fixed flow rate (250 µL/min) using a syringe. The tube, made of a biocompatible silicone, was positioned in degassed water at a distance of 12.5 mm from the probe surface.

To perform superharmonic imaging, a 4-cycle burst centered at 3 MHz was transmitted on the LF element with a peak negative pressure of 500 kPa (mechanical index = 0.29). The number of cycles (i.e., 4 cycles) was chosen to preserve the axial resolution. For imaging, the transducer was mounted on an XYZ-positioning system controlled by Matlab (Fig. 7). The ultrasound image was built using a mechanical scan with a step of 50 µm. The resulting image is composed of 41 RF lines acquired using the HF transducer. Echoes were filtered from 8 to 18 MHz (Matlab, Butterworth filter, order 3) to isolate the superharmonic components.

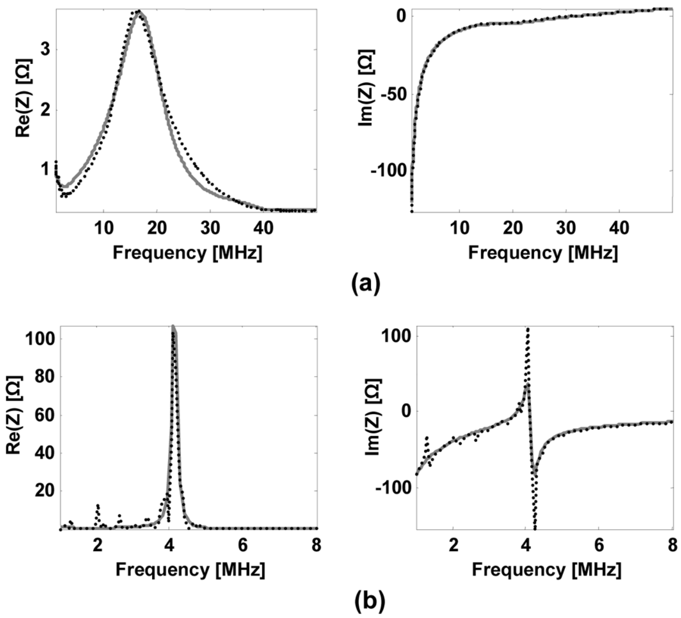

Fig. 8. Experimental (black dotted lines) and theoretical (gray solid lines) impedance (real and imaginary parts) of (a) high-frequency (HF) element and (b) low-frequency (LF) element in air.

IV. Results and Discussion

A. Functional Properties of Piezoelectric Elements

In Fig. 8, electrical impedances calculated with the KLM scheme (gray solid lines) are compared with the experimental curves (black dotted lines) for the two elements around the resonant frequencies. All the fixed input data used for the fitting process are summarized in Table I (acoustic, physical, and geometrical properties). Fig. 8(a) displays the results for the HF element; Fig. 8(b) corresponds to the LF element. The deduced parameters exhibit good electromechanical performance with thickness coupling factors of 44% and 46% for the HF and LF elements, respectively. These values are comparable to those obtained with standard bulk ceramics (typically plane disk) with the same compositions. Moreover, the porosity content in the HF element leads to a decrease of density but also longitudinal wave velocity [19], and consequently the corresponding acoustic impedance is relatively

TABLE I. Characteristics of Each Constitutive Element of the Transducer.

Transducer component	Material	t (µm)	ρ (kg/m^3)	v_l (m/s)	Z (MRa)	$\varepsilon_{33}^S/\varepsilon_0$	k_t (%)	δ_m (%)
Backing	Porous PZT	10000	5800	2700	15.6	—	—	—
HF element	PZT	43	6600	*2150*	*14.2*	*315*	*44*	*3*
LF element	PZT Pz26	502	7700	*4250*	*33.6*	*630*	*46*	*4*
Top electrode	HF: Ag	2	10500	3600	37.8	—	—	—
	LF: Ag	4						
Bottom electrode	HF: Au	3	19600	3240	63.8	—	—	—
	LF: Ag	4	10500	3600	37.8			

t = thickness, ρ = density, v_l = longitudinal wave velocity, Z = acoustic impedance, $\varepsilon_{33}^S/\varepsilon_0$ = dielectric constant at constant strain (measured at f_a), k_t = effective thickness coupling factor, δ_m = mechanical losses. Italic parameters were deduced for the fitting process with the Krimholtz–Leedom–Matthaei (KLM) model.

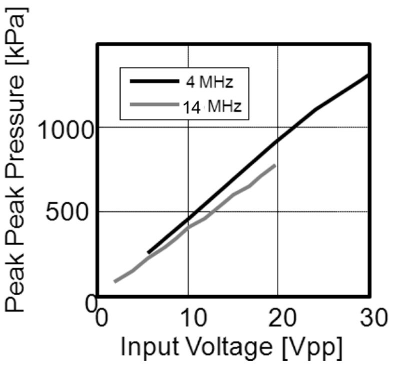

Fig. 9. Acoustic pressure (in kilopascals) at focal point versus input voltage (in volts) for both elements.

low (14.5 MRa). This allows delivery of a better acoustical matching between the PZT thick film and the propagation medium (water or tissue). All of these deduced parameters for the two elements are given in italic text in Table I.

B. Transducer Acoustic Characteristics

The sensitivities of both LF and HF elements are shown in Fig. 9. For that, acoustic pressures measured at the focal distance for different values of input voltage (10-cycle burst excitation at the center frequency of each element was used) are given for the LF element (4 MHz) and the HF element (14 MHz). A fairly linear pressure-versus-voltage curve with no saturation was observed for the two transducer elements. Additional measurements were performed on a similar curved thick film, and an acoustic pressure of 3 MPa can be achieved for an input voltage over 140 V_{pp} [14].

Again, all the data given in Table I are used for the modeling. Acoustic pressure fields for both elements were calculated independently with the PS-FDTD model coupled with the DREAM toolbox. Fig. 10(a) represents the normalized pressure field in the z-axis and the measured focal distance corresponds to the radius of curvature of the two elements (maxima of the normalized pressure field). For the LF element, this value is slightly higher, around 500 μm, which corresponds to the thickness of the element that is directly glued onto the curved substrate. Finally, the estimated focal distances are 12.2 and 12.7 mm for the HF and LF elements, respectively. The depth of field at −3 dB is deduced from both experimental and theoretical results. These values are given in Table II. Fig. 10(b) shows the normalized pressure in the x-axis (perpendicular to the z-axis, Fig. 6) at the two focal distances. The lateral resolutions (at −3 dB) for the two elements are

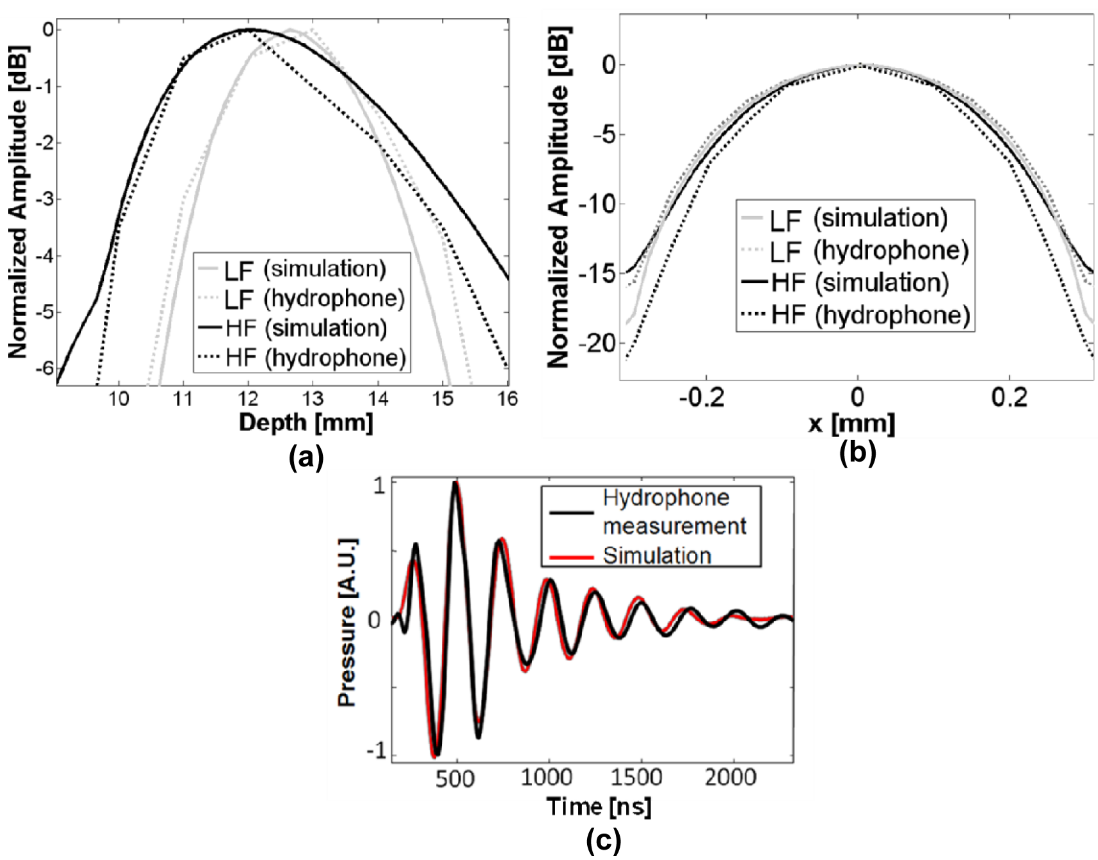

Fig. 10. Theoretical and experimental radiation pattern characteristics for both elements (normalized pressure field): (a) for depth of field in the z-axis, (b) in the plane perpendicular of the z-axis at the focal distance of the two elements (for lateral resolutions), (c) electro-acoustic response of the LF element at the focal distance (12.7 mm).

TABLE II. Results and Comparison of Hydrophone Measurement/Simulation.

	Outer LF element	Center HF element
Center frequency (MHz)	4/4	13.5/13.7
−3-dB Bandwidth (%)	18/16	67/71
−3-dB Axial resolution (μm)	610/630	84/92
−3-dB Lateral resolution (μm)	310/300	250/280
−3-dB Depth of field (mm)	3.7/3.2	4.6/5.1

LF = low frequency, HF = high frequency.

around 300 μm (Table II). Finally, with one-cycle burst excitation at the center frequency of each element, the electro-acoustic response was measured and calculated at the focal point. Fig. 10(c) shows the results for the LF element. From these results, the axial resolution (−3 dB) and the fractional bandwidth (−3 dB) are deduced (Table II). As expected, the bandwidth of the HF center element is high and approaches 70%, whereas for the outer LF element, this value is less than 20%. For the three figures, the theoretical results are in good agreement with the measurements, where the largest observed differences are around 20 μm for the axial resolution, 0.5 mm for the depth of field, and 30 μm for the lateral resolution (which represents a relative variation of around 10%). The numerical model used is an efficient tool to predict the radiation pattern of piezoelectric transducers with complex shapes.

C. Detection and Imaging of Superharmonic Components

Spectra of the averaged responses of BR14 microbubbles are displayed in Fig. 11. The results were normalized by the HF transducer bandwidth. In this case, the LF transducer was used in transmit and the HF transducer in receive mode. In this example, the fourth harmonic component (12 MHz) is close to the center frequency of the HF element. The figure shows that the bandwidth of the HF element is wide enough to detect five harmonic components (from second to sixth harmonic) of the microbubbles. No harmonics are detected from the linear reflector. This result confirms that the superharmonic components observed from the response of microbubbles are not caused by undesirable transducer intrinsic effects and frequency interaction between the two elements and/or nonlinear propagation effects.

The corresponding SNR for each frequency component is given in Table III. An SNR ranging from 7 to 18 dB was detected for the superharmonic components. Using traditional PZT transducers (with only one element), these higher harmonics are not detectable because of the lack of sensitivity induced by the bandwidth (70% to 80%). In fact, for this application, a transducer fractional bandwidth higher than 130% is required. One solution is to use other transducer technologies offering a wide frequency bandwidth, such as PVDF or cMUT transducers. Nevertheless, as a transmitter, the PVDF-based transducer can suffer from a lack of sensitivity for medical applications [36]. More recently, cMUTs have also emerged as a good alternative to PZT transducers but the influence of their inherent nonlinear behavior on superharmonic imaging must first be investigated [37]. In this context, the development of a dual-frequency transducer made with PZT materials seems to be the most adapted approach so far.

TABLE III. SNR for Superharmonic Components.

Harmonic	2nd	3rd	4th	5th	6th
Frequency (MHz)	6	9	12	15	18
SNR (dB)	25	18	15	10	7

Finally, the transducer has been evaluated *in vitro* for superharmonic contrast imaging. Images of a tube containing water [Fig. 12(a)] and a diluted solution of microbubbles [Fig. 12(b)] were recorded using a mechanical scan. Each figure is displayed with a dynamic range of 25 dB. In Fig. 12(a), no superharmonic response is measured in the phantom, where the tube outline is represented by the dotted circle. This demonstrates that there is no nonlinear reflection from the tube at high harmonic frequencies. After addition of contrast agent, one can see the echo enhancement revealing the circulating microbubbles inside the tube [Fig. 12(b)]. This study indicates that superharmonic imaging can be successfully performed at higher frequency (e.g., 9 to 18 MHz) compared with previous studies from Bouakaz *et al.* [38] and Van Neer *et al.* [10] (2.4 to 5 MHz). This result opens new opportunities in high-resolution contrast superharmonic imaging.

V. Conclusions

A new dual-frequency transducer was designed and successfully fabricated using pad-printing technology for the HF element, whereas for the LF, a curved ring shape was

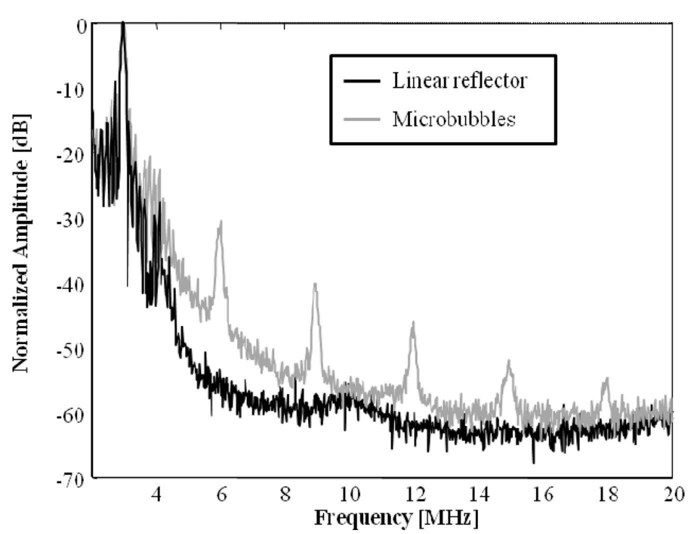

Fig. 11. Superharmonic frequency response from linear reflector and microbubbles.

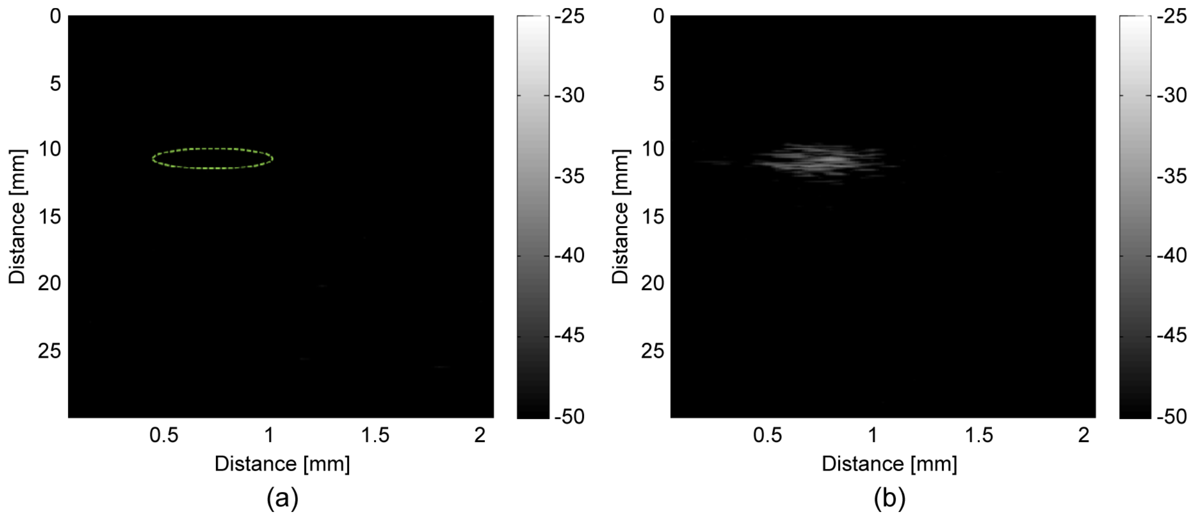

Fig. 12. Superharmonic imaging of a flow phantom containing (a) water and (b) contrast agent microbubbles. The circle corresponds to the tube position.

obtained by machining and gluing onto a common porous PZT substrate. One of the main objectives was to develop a simple process for efficient transducers. The electromechanical performance of the two piezoelectric elements was high and comparable to standard bulk ceramic with similar compositions (typically a thickness coupling factor around 45% for both elements). The acoustic characterization of the transducer in water confirmed that the two elements have the same focal distance (around 12.5 mm). The sensitivity was emphasized for the outer ring (typically 1.3 MPa for 30 V) and a linear response of the pressure was measured for a wide range of input voltages. For the center element, priority was given to the fractional bandwidth (70% at −3 dB), which allowed a wide frequency range (from 3 to 20 MHz) to be covered. These results were theoretically confirmed using a numerical model specifically adapted for a curved piezoelectric structure.

By choosing the same focal area for the two elements, the experimental setup was greatly simplified and was successfully used for superharmonic imaging. A contrast agent solution (with BR14 microbubbles) was used in a flow phantom (tube) positioned at the focal distance and five harmonic components (from second to sixth) were detected with good sensitivity (SNR ranging from 7 to 18 dB). The corresponding imaging confirmed these results.

Finally, this fabricated transducer specifically designed for high-frequency superharmonic detection confirmed this possibility (here, up to 20 MHz) and opens new fields of interest such as monitoring of superficially located cancer lesions.

Acknowledgments

The authors thank Bracco Research, Geneva, for supplying contrast agent, and J.-Y. Tartu for his technical support.

References

[1] S. R. Wilson and P. N. Burns, "Microbubble-enhanced US in body imaging: What role?" *Radiology*, vol. 257, pp. 24–39, Oct. 2010.

[2] N. de Jong, A. Bouakaz, and F. J. Ten Cate, "Contrast harmonic imaging," *Ultrasonics*, vol. 40, pp. 567–573, May 2002.

[3] F. Forsberg, W. T. Shi, and B. B. Goldberg, "Subharmonic imaging of contrast agents," *Ultrasonics*, vol. 38, pp. 93–98, Mar. 2000.

[4] J. R. Eisenbrey, J. K. Dave, V. G. Halldorsdottir, D. A. Merton, P. Machado, J. B. Liu, C. Miller, J. M. Gonzalez, S. Park, S. Dianis, C. L. Chalek, K. E. Thomenius, D. B. Brown, V. Navarro, and F. Forsberg, "Simultaneous grayscale and subharmonic ultrasound imaging on a modified commercial scanner," *Ultrasonics*, vol. 51, pp. 890–897, Dec. 2011.

[5] Y. Sun, D. E. Kruse, P. A. Dayton, and K. W. Ferrara, "High-frequency dynamics of ultrasound contrast agents," *IEEE Trans. Ultrason. Ferroelectr. Freq. Control*, vol. 52, pp. 1981–1991, Nov. 2005.

[6] A. Bouakaz, S. Frigstad, F. J. Ten Cate, and N. de Jong, "Improved contrast to tissue ratio at higher harmonics," *Ultrasonics*, vol. 40, pp. 575–578, May 2002.

[7] A. Bouakaz, B. J. Krenning, W. B. Vletter, F. J. ten Cate, and N. De Jong, "Contrast superharmonic imaging: A feasibility study," *Ultrasound Med. Biol.*, vol. 29, pp. 547–553, Apr. 2003.

[8] H. H. Kim, J. M. Cannata, R. Liu, J. H. Chang, R. H. Silverman, and K. K. Shung, "20 MHz/40 MHz dual element transducers for high frequency harmonic imaging," *IEEE Trans. Ultrason. Ferroelectr. Freq. Control*, vol. 55, pp. 2683–2691, Dec. 2008.

[9] S. E. Masoy, O. Standal, P. Nasholm, T. F. Johansen, B. Angelsen, and R. Hansen, "SURF imaging: In vivo demonstration of an ultrasound contrast agent detection technique," *IEEE Trans. Ultrason. Ferroelectr. Freq. Control*, vol. 55, pp. 1112–1121, May 2008.

[10] P. L. van Neer, G. Matte, M. G. Danilouchkine, C. Prins, F. van den Adel, and N. de Jong, "Super-harmonic imaging: Development of an interleaved phased-array transducer," *IEEE Trans. Ultrason. Ferroelectr. Freq. Control*, vol. 57, pp. 455–468, Feb. 2010.

[11] R. Gessner, M. Lukacs, M. Lee, E. Cherin, F. S. Foster, and P. A. Dayton, "High-resolution, high-contrast ultrasound imaging using a prototype dual-frequency transducer: In vitro and in vivo studies," *IEEE Trans. Ultrason. Ferroelectr. Freq. Control*, vol. 57, pp. 1772–1781, Aug. 2010.

[12] E. Filoux, S. Calle, D. Certon, M. Lethiecq, and F. Levassort, "Modeling of piezoelectric transducers with combined pseudospectral and finite-difference methods," *J. Acoust. Soc. Am.*, vol. 123, pp. 4165–4173, Jun. 2008.

[13] E. Filoux, S. Calle, R. Lou-Moeller, M. Lethiecq, and F. Levassort, "3-D numerical modeling for axisymmetrical piezoelectric structures: Application to high-frequency ultrasonic transducers," *IEEE Trans. Ultrason. Ferroelectr. Freq. Control*, vol. 57, pp. 1188–1199, May 2010.

[14] E. Filoux, R. Lou-Moeller, S. Callé, M. Lethiecq, and F. Levassort, "Optimised properties of high frequency transducers based on curved piezoelectric thick films obtained by pad printing process," *Adv. Appl. Ceram.*, vol. 112, pp. 75–78, Feb. 2013.

[15] M. Lethiecq, R. Lou-Moeller, J. Ketterling, F. Levassort, L. P. Tran-Huu-Hue, E. Filoux, R. H. Silverman, and W. W. Wolny, "Non-planar pad-printed thick-film focused high-frequency ultrasonic transducers for imaging and therapeutic applications," *IEEE Trans. Ultrason. Ferroelectr. Freq. Control*, vol. 59, pp. 1976–1982, Sep. 2012.

[16] F. A. Duck, "Nonlinear acoustics in diagnostic ultrasound," *Ultrasound Med. Biol.*, vol. 28, pp. 1–18, Jan. 2002.

[17] J. M. Escoffre, A. Novell, J. Piron, A. Zeghimi, A. Doinikov, and A. Bouakaz, "Microbubble attenuation and destruction: Are they involved in sonoporation efficiency?" *IEEE Trans. Ultrason. Ferroelectr. Freq. Control*, vol. 60, pp. 46–52, Jan. 2013.

[18] D. Chatterjee, K. Sarkar, P. Jain, and N. E. Schreppler, "On the suitability of broadband attenuation measurement for characterizing contrast microbubbles," *Ultrasound Med. Biol.*, vol. 31, pp. 781–786, Jun. 2005.

[19] F. Levassort, J. Holc, E. Ringgaard, T. Bove, M. Kosec, and M. Lethiecq, "Fabrication, modelling and use of porous ceramics for ultrasonic transducer applications," *J. Electroceram.*, vol. 19, pp. 125–137, Sep. 2007.

[20] P. Marechal, F. Levassort, J. Holc, L. P. Tran-Huu-Hue, M. Kosec, and M. Lethiecq, "High-frequency transducers based on integrated piezoelectric thick films for medical imaging," *IEEE Trans. Ultrason. Ferroelectr. Freq. Control*, vol. 53, pp. 1524–1533, Aug. 2006.

[21] InSensor AS. (2013, Oct.) TF2100 PZT thick film based on Ferroperm Pz26. [Online]. Available: http://www.insensor.com/download/files/1234182533.pdf

[22] R. Krimholtz, D. A. Leedom, and G. L. Matthaei, "New equivalent circuit for elementary piezoelectric transducers," *Electron. Lett.*, vol. 6, pp. 398–399, Jun. 25, 1970.

[23] S. J. H. Van Kervel and J. M. Thijissen, "A calculation scheme for the optimum design of ultrasonic transducers," *Ultrasonics*, vol. 21, pp. 134–140, May 1983.

[24] L. P. Tran-Huu-Hue, F. Levassort, N. Felix, D. Damjanovic, W. Wolny, and M. Lethiecq, "Comparison of several methods to characterise the high frequency behaviour of piezoelectric ceramics for transducer applications," *Ultrasonics*, vol. 38, pp. 219–223, Mar. 2000.

[25] M. Lukacs, T. Olding, M. Sayer, R. Tasker, and S. Sherrit, "Thickness mode material constants of a supported piezoelectric film," *J. Appl. Phys.*, vol. 85, pp. 2835–2843, Mar. 1999.

[26] A. Bardaine, P. Boy, P. Belleville, O. Acher, and F. Levassort, "Improvement of composite sol-gel process for manufacturing 40-μm piezoelectric thick films," *J. Eur. Ceram. Soc.*, vol. 28, pp. 1649–1655, 2008.

[27] A. R. Selfridge, "Approximate material properties in isotropic materials," *IEEE Trans. Sonics Ultrason.*, vol. 32, pp. 381–394, 1985.

[28] F. Lingvall, "Time-domain reconstruction methods for ultrasonic array imaging," Ph.D. thesis, Signals and Systems Dept., Uppsala University, Uppsala, Sweden, 2004.

[29] H. O. Kreiss and J. Oliger, "Comparison of accurate methods for the integration of hyperbolic equations," *Tellus*, vol. 24, pp. 199–215, Jun. 1972.

[30] G. Wojcik, B. Fornberg, R. Waag, L. Carcione, J. Mould, L. Nikodym, and D. A. Driscoll, "Pseudospectral methods for large-scale bioacoustic models," in *Proc. IEEE Ultrasonics Symp.*, 1997, pp. 1501–1506.

[31] B. Fornberg, "The pseudospectral method: Comparisons with finite differences for the elastic wave equation," *Geophysics*, vol. 52, pp. 483–501, Apr. 1987.

[32] Q. H. Liu, "The PSTD algorithm: A time-domain method requiring only two cells per wavelength," *Microw. Opt. Technol. Lett.*, vol. 15, pp. 158–165, Jun. 1997.

[33] J. P. Berenger, "A perfectly matched layer for the absorption of electromagnetic waves," *J. Comput. Phys.*, vol. 114, pp. 185–200, Oct. 1980.

[34] S. Calle, J. P. Remenieras, M. Elkateb, and F. Patat, "Shear wave elastography: Modeling of the shear wave propagation in heterogeneous tissue by pseudospectral method," in *Proc. IEEE Ultrasonics Symp.*, 2004, pp. 24–27.

[35] E. Filoux, F. Levassort, S. Calle, D. Certon, and M. Lethiecq, "Theoretical analysis of single element transducer using a hybrid FD-PSTD model," *Ultrasonics*, vol. 49, pp. 611–614, Dec. 2009.

[36] C. Z. Rosen and B. V. Hiremath, *Piezoelectricity.* New York, NY: American Institute of Physics, 1992.

[37] A. Novell, M. Legros, N. Felix, and A. Bouakaz, "Exploitation of capacitive micromachined transducers for nonlinear ultrasound imaging," *IEEE Trans. Ultrason. Ferroelectr. Freq. Control*, vol. 56, pp. 2733–2743, Dec. 2009.

[38] A. Bouakaz, S. Frigstad, F. J. Ten Cate, and N. de Jong, "Super harmonic imaging: A new imaging technique for improved contrast detection," *Ultrasound Med. Biol.*, vol. 28, pp. 59–68, Jan. 2002.

Axel Guiroy received a master's degree in biomechanics from the Louis Pasteur University of Strasbourg, France. From 2005 to 2008, he did research on the mechanics of a single living cell in the Complex Matter and System laboratory (MSC) of Denis Diderot University, Paris, France. He received a Ph.D. degree in 2008. In 2010, he joined the laboratories Imagerie and Cerveau, INSERM U930, and GREMAN CNRS 7347, at the University François-Rabelais in Tours, France, where he carried out research on piezoelectric acoustic modeling and bubble detection. He currently holds a postdoctoral position at the Langevin Institute, Paris, France, where he studies scuba divers' decompression sickness. His interests include bubble detection and transducer design.

Anthony Novell received his M.Sc. degree in medical imaging technologies in 2007 and his Ph.D. degree in 2011 from the University François Rabelais, Tours, France. He is currently pursuing his postdoctoral research at the French Institute for Health and Medical Research (Inserm) in Tours, France. His research focuses on contrast agent imaging, capacitive micromachined ultrasonic transducers (cMUTs), and therapeutic ultrasound.

Erling Ringgaard is an R&D Project Manager of Meggitt A/S and has more than 15 years of experience in the field of piezoelectric ceramics. He holds an M.Sc. degree in chemistry and a Ph.D. degree in materials science. He has authored or co-authored more than 60 scientific papers and conference articles. He has participated in a number of EC-funded RTD projects and been the coordinator of two of these. Currently, he is the project leader of a nationally funded project on energy harvesting.

Rasmus Lou-Møller received an M.S. degree in applied physics from the Technical University of Denmark in 2003. He is currently a project manager in Ferroperm Piezoceramics in Denmark. Since 2004, he has been working on the development of piezoceramic thick films and applications utilizing this technology.

Jean-Marc Grégoire was born in Paris, France, in 1957. He studied electronics and in 1981, he joined the SKF Company, where he was employed as an electronic technician at the Experimentation Laboratory for the development of machines for nuclear industry. From 1982 to 1985, he was support technician to X-ray and ultrasound medical systems for Philips Medical Systems (Massiot-Philips). In 1986, he joined the University Francois-Rabelais of Tours, where his tasks focus on the development of electronic systems for ultrasonic medical applications to the Laboratory for Ultrasound Systems Instrumentation (LUSSI).

He obtained his electronic engineering degree from the Conservatoire National des Arts et Metiers of Tours, France, in 1995, and he received the Ph.D. degree in sciences of life and health from the University François-Rabelais of Tours, France, in 2002 on high-resolution ultrasound imaging systems from 10 to 50 MHz.

After receiving his Ph.D. degree, he was promoted to a research engineer for the Laboratory Imagerie and Cerveau (Imaging and Brain) where he developed a great number of 2-D and 3-D mechanical probes with specific electronics for high-resolution imaging. He recently designed a high-frequency (20 to 50 MHz) real-time beamformer with 128 to 256 channels.

André-Pierre Abellard was born in France in 1986. He received his M.Sc. degree in nonlinear phenomena from the François-Rabelais University of Tours, France, in 2010. Since 2010, he has been a Ph.D. student at François Rabelais University of Tours and the Jozef Stefan Institute, Ljubljana, Slovenia. His research focuses on transducer development and piezoelectric material.

Tomasz Zawada holds a Ph.D. degree in microelectronic engineering, an M.Sc. degree in electronic engineering, and an M.B.A. degree in management of technology. Tomasz has more than 10 years of experience in academic and industrial research in the fields of ceramic microsystems, microfluidics, and piezoelectric materials and devices. He has authored or co-authored more than 60 scientific publications and reports. Currently, he is working as Engineering and Research Manager at Meggitt A/S, Denmark. His main professional interest is focused on applications of piezoelectric thick films in sensors, transducers, and energy harvesting.

Ayache Bouakaz graduated from the University of Sétif, Algeria, from the Department of Electrical Engineering. He obtained his Ph.D. degree in 1996 from the Department of Electrical Engineering at the Institut National des Sciences Appliquées de Lyon (INSA Lyon), France. In 1998, he joined the Department of Bioengineering at The Pennsylvania State University in State College, PA, where he worked in a postdoctoral position for 1 year. From February 1999 to November 2004, he was employed at the Erasmus University Medical Center, Rotterdam, The Netherlands. His research focused on imaging, ultrasound contrast agents, and transducer design. Since January 2005, he has held a permanent position as a director of research at the French Institute for Health and Medical Research, INSERM, in Tours, France. His research focuses on imaging and therapeutic applications of ultrasound and microbubbles.

Franck Levassort was born in 1968 near Paris, France. He graduated in Applied Physics in 1990 and received the D.E.A. degree in physical acoustics from University Paris 7 (Denis Diderot) in 1991. In 1996, he received the Ph.D. degree in ultrasound from the University François-Rabelais of Tours, France. Since 1997, he has been Assistant Professor of Mechanical and Materials Engineering at the University François-Rabelais, Institute of Technology, Blois, France,

His current interests are in design, modeling and characterization of piezoelectric composite materials and structures, as well as transducers for imaging applications.

He is a member of the French Society of Acoustics and the Acoustical Society of America.